Journal of Sound and Vibration (1999) **226**(5), 1029–1042
Article No. jsvi.1999.2340, available online at http://www.idealibrary.com on IDEAL®

DAMAGE DETECTION USING THE FREQUENCY-RESPONSE-FUNCTION CURVATURE METHOD

R. P. C. SAMPAIO

Departamento de máquinas Marítimas, Escola Náutica Infante, D. Henrique, Av. Eng Bonneville Franco, Paço d'Arcos, 2780 *Oeiras, Portugal*

AND

N. M. M. MAIA AND J. M. M. SILVA

Departamento de Engenharia Mecanica, Instituto Superior Técnico, av. Rovisco Pais, 1096 *Lisboa Codex, Portugal*

(*Received* 9 *October* 1998, *and in final form* 19 *April* 1999)

Structural damage detection has gained increasing attention from the scientific community since unpredicted major hazards, most with human losses, have been reported. Aircraft crashes and the catastrophic bridge failures are some examples. Security and economy aspects are the important motivations for increasing research on structural health monitoring. Since damage alters the dynamic characteristics of a structure, namely its eigenproperties (natural frequencies, modal damping and modes of vibration), several techniques based on experimental modal analysis have been developed in recent years. A method that covers the four steps of the process of damage detection—existence, localization, extent and prediction—has not yet been recognized or reported. The frequency-response-function (FRF) curvature method encompasses the first three referred steps being based on only the measured data without the need for any modal identification. In this paper, the method is described theoretically and compared with two of the most referenced methods on literature. Numerically generated data, from a lumped-mass system, and experimental data, from a real bridge, are used for better illustration.

1. INTRODUCTION

Higher operational loads, greater complexity of design and longer lifetime periods imposed to civil, mechanical and aerospace structures, make it increasingly important to monitor the health of these structures. A wide variety of highly effective non-destructive methods, using strain gauges, penetrating liquids, ultra-sound, visual inspection, etc., are currently available for the detection of defects. Unfortunately, they are all localized techniques, implying long and expensive inspection time; often, structural components are not inspected just because of their inaccessibility and damage can propagate to critical levels between the inspection intervals.

0022-460X/99/401029 + 14 $30.00/0

The drawbacks of current inspection techniques have led engineers to investigate new methods for continuous monitoring and global condition assessment of structures. That is the case for methods based on vibration responses that allow one to obtain meaningful time and/or frequency domain data and calculate changes in the structural and modal properties, such as resonance frequencies, modal damping and mode shapes, and use them with the objective of developing reliable techniques to detect, locate and quantify damage.

In the past 20 years a lot of work has been published in the area of damage detection, where various methods have been proposed. A comprehensive survey on damage detection and evaluation methods is given in reference [1]. However, there are still a lot of problems [2–4] that need more insight such as the following: testing variability of the measured data (noise, test set-up, ...); using ambient vibration as input source; sensitivity of the methods (small defects only produce small changes in the modal parameters); different defects could be responsible for the same changes in the eigenparameters (non-uniqueness); assessment of the extension of damage; prediction of the remaining useful life.

When damage occurs in a structure the consequence is a change in one or more of its dynamic properties, namely the stiffness, mass or damping. If one is referring to cracks, then it may be assumed that there will be a detectable change in stiffness, the mass remaining unchanged and, in a first approximations, that the change in damping may be disregarded. In such a situation, our attention is focused on monitoring changes in the stiffness. This is the case that will be addressed in the method presented and discussed in this paper.

2. THEORETICAL DESCRIPTION

For a better understanding of the method, it was decided to compare it with two other relevant methods referenced in the literature—the Mode Shape Curvature method [5] and the Damage Index method [6.]

2.1. THE MODE SHAPE CURVATURE METHOD

Pandey, *et al.* [5] stated that once the mode shapes of a damaged and of the corresponding undamaged structure (respectively $\{\phi_d\}$ and $\{\phi\}$) are identified, the curvature at each location i on the structure is numerically obtained by a central difference approximation:

$$\phi_i'' = (\phi_{i+1} - 2\phi_i + \phi_{i-1})/h^2 , \tag{1}$$

where h is the distance between the measurement points $i + 1$ and $i - 1$.

The location of the damage is then assessed by the largest computed absolute difference between the mode shape curvatures of the damaged and undamaged structure, as follows:

$$\{\Delta\phi''\} = |\{\phi_d''\} - \{\phi''\}|. \tag{2}$$

2.2. THE DAMAGE INDEX METHOD

Stubbs and Kim [6] proposed a damage index, based on the changes in the curvature of the jth mode at location i, defined as

$$\beta_{i,j} = \frac{\left(\int_a^b [\phi_j^{d\prime\prime}(x)]^2 \, \mathrm{d}x + \int_0^L [\phi_j^{d\prime\prime}(x)]^2 \, \mathrm{d}x \right) \int_0^L [\phi_j''(x)]^2 \, \mathrm{d}x}{\left(\int_0^b [\phi_j''(x)]^2 \, \mathrm{d}x + \int_0^L [\phi_j''(x)]^2 \, \mathrm{d}x \right) \int_0^L [\phi_j^{d\prime\prime}(x)]^2 \, \mathrm{d}x}, \tag{3}$$

where $\phi_j''(x)$ and $\phi_j^{d\prime\prime}(x)$ are the second derivatives of the jth mode shape corresponding to the undamaged and damaged structures, respectively, L is the length of the structure, a (location i) and b (location $i+1$) are the limits of a segment of the structure where damage is being evaluated. The mode shape functions of x are evaluated by fitting the measured data with a cubic polynomial. If more than one mode is used, the damage index is the sum of the damage indices from each mode:

$$\nu_i = \sum_j \beta_{i,j} \, . \tag{4}$$

Statistical methods are then used to examine the changes in the damage index and associate these changes with the possible damage locations. A normal distribution is fit to the damage indices, and values falling two or more standard deviations from the mean are assumed to be the most likely location of damage [7].

For the purpose of this paper it was decided to use the following formulation of the Damage index method:

$$\beta_{i,j} = \frac{\left(\{\phi_d''\}_{i,j}^2 + \sum_1^{i_{\max}} \{\phi_d''\}_{i,j}^2 \right) \cdot \sum_1^{i_{\max}} \{\phi''\}_{i,j}^2}{\left(\{\phi''\}_{i,j}^2 + \sum_1^{i_{\max}} \{\phi''\}_{i,j}^2 \right) \cdot \sum_1^{i_{\max}} \{\phi_d''\}_{i,j}^2}. \tag{5}$$

Here $i$max is the maximum order location.

2.3. THE FREQUENCY RESPONSE FUNCTION (FRF) CURVATURE METHOD

Basically, this method is an extension of the Pandey *et al.* method to all frequencies in the measurement range and not just the modal frequencies; i.e., it uses FRF data rather than just mode shape data. In fact, the method uses something like an "operational mode shape" defined, for each frequency, by the frequency response at the different locations of the structure.

The curvature for each frequency is given by

$$\alpha''(\omega)_{i,j} = \frac{\alpha(\omega)_{i+1,j} - 2\alpha(\omega)_{i,j} + \alpha(\omega)_{i-1,j}}{h^2}, \tag{6}$$

where $\alpha_{i,j}$ is the receptance FRF measured at location i for a force input at location j.

The absolute difference between the FRF curvatures of the damaged and undamaged structure at location i, along the chosen frequency range, is calculated, for an applied force at point j, by

$$\Delta\alpha''_{i,j} = \sum_{\omega} |\alpha''_d(\omega)_{i,j} - \alpha''(\omega)_{i,j}|. \tag{7}$$

Finally, one can sum up for several force location cases:

$$S_i = \sum_j \Delta\alpha''_{i,j}. \tag{8}$$

As will be seen from the numerical and experimental results, this method can detect, localize and assess damage extent.

3. NUMERICAL EXAMPLES

For the examples that follow, simulated data obtained for a bending a free–free beam were generated by using an equivalent spring–mass system of 10 degrees-of-freedom (DOF) without damping. The finite element method was not used as in reference [3], as the same conclusions can be drawn from the spring–mass system, much less time-consuming and easier for the analysis.

It is assumed that neither the location nor the characteristics of the damaged zone are known. This is generally the case in practical vibration monitoring, where both the location and size of the damage are unknown. It was decided to model the change in the stiffness of the damaged element (between two consecutives measurement points) as a percentage reduction of the undamaged one. To circumvent numerical problems associated with this model, it was also decided to reduce the masses by a very small amount (about 0·01%).

For comparison purposes a model of 10 masses with 1 kg each and nine springs with 10 000 N/m each (see Figure 1) was used. Four levels of damage at the same location were considered. The damage was introduced between the measurement points 4 and 5 (masses 4 and 5) modeled by 0·01% mass reduction of each of these masses and by 20, 40, 60 and 80% stiffness reduction of spring 4; this corresponds, respectively, to the damage level situations d1, d2, d3 and d4.

3.1. THE FRF CURVATURE METHOD

Figure 2 shows some FRFs of the damaged and undamaged model, plotted for a frequency range of 0–200 rad/s, measured on location 1 for an input force on the same location.

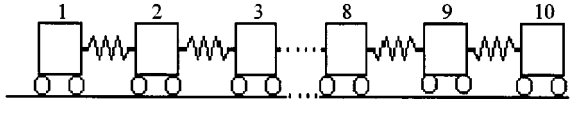

Figure 1. Lumped-mass model of 10 degrees-of-freedom. Keys: ——, 20% damage; ———, 80% damage; – – – , undamaged.

Figure 3 plots of the method and one can see its high performance concerning the localization and damage quantification.

3.1.1. *Influence of the frequency range*

While testing different frequency intervals it was found that the method worked better for a range before the first anti-resonance or resonance (whichever comes first). In fact, for wider frequency ranges, including several modes, the difference of curvatures of the damaged and undamaged model becomes less significant when compared with the amplitude difference arising from the reasonances' frequency shift, because of the loss of stiffness, The result is therefore less reliable in detecting and estimating the damage extent. This conclusion is obvious from the observation of Figures 4–6.

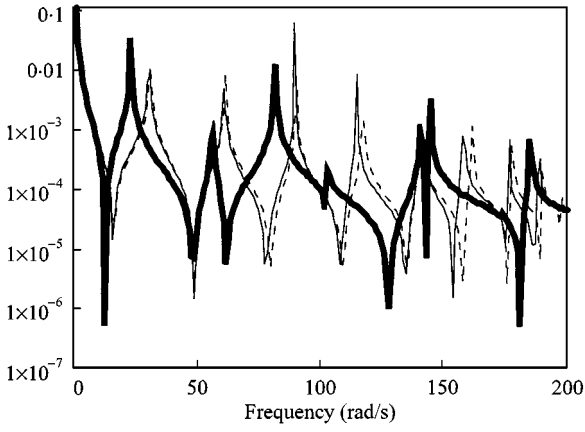

Figure 2. Receptance FRFs of the undamaged and damaged model, measured at point 1 for an input force at the same point. Keys: ——, 20% damage (between measurement points 4 and 5); ——, 40% damage (between measurement points 4 and 5); ▬, 60% damage (between measurement points 4 and 5); ▬, 80% damage (between measurement points 4 and 5).

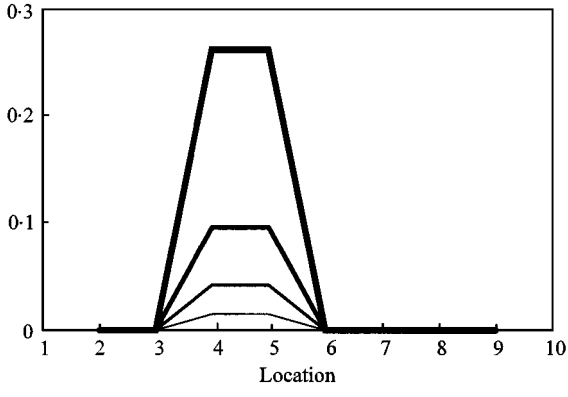

Figure 3. FRFs curvature differences for a frequency range of 0–10 rad/s. Input force at location 1. Keys: ——, 20% damage (between measurement points 4 and 5); ——, 40% damage (between measurement points 4 and 5); ▬, 60% damage (between measurement points 4 and 5); ▬, 80% damage (between measurement points 4 and 5).

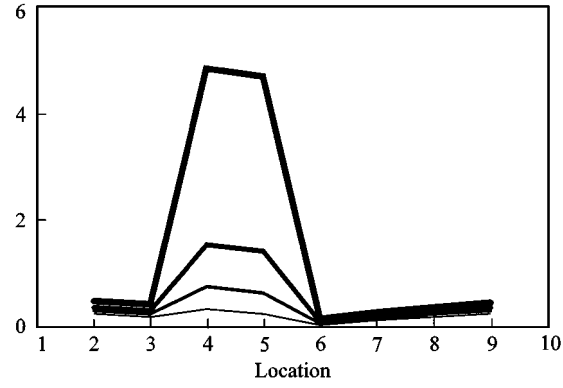

Figure 4. FRFs curvature differences for a frequency range of 0–50 rad/s. Input force at location 1. Keys: ——, 20% damage (between measurement points 4 and 5); ——, 40% damage (between measurement points 4 and 5); ▬, 60% damage (between measurement points 4 and 5); ▬, 80% damage (between measurement points 4 and 5).

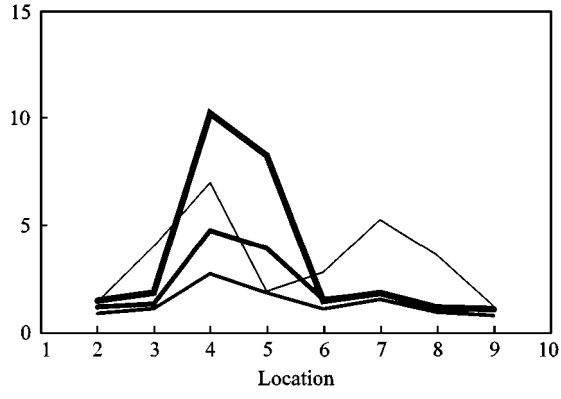

Figure 5. FRFs curvature differences for a frequency range of 0–100 rad/s. Input force at location 1. Keys: ——, 20% damage (between measurement points 4 and 5); ——, 40% damage (between measurement points 4 and 5); ▬, 60% damage (between measurement points 4 and 5); ▬, 80% damage (between measurement points 4 and 5).

3.1.2. *Influence of the input force location*

It was also found that it was necessary to assess the influence of the input force location on the results. From Figure 7, for the damage situation d4, it seems that the influence of the position of the exciting force is not important. The same conclusion was found in a previous work [3].

3.1.3. *Influence of noise*

To determine the influence of adding the noise to the numerical data (noise is always present on experimental data) it was decided to pollute our model's data with a multiplicative error of 10% of rms. Figure 8 shows that this method is quite is quite insensitive to noise.

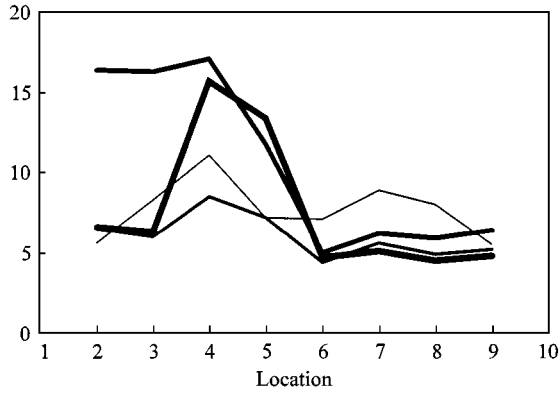

Figure 6. Frequency range of 0–200 rad/s: Keys: ––20% damage (between measurement points 4 and 5);——, 40% damage (between measurement points 4 and 5); ▬, 60% damage (between measurement points 4 and 5); ▬, 80% damage (between measurement points 4 and 5).

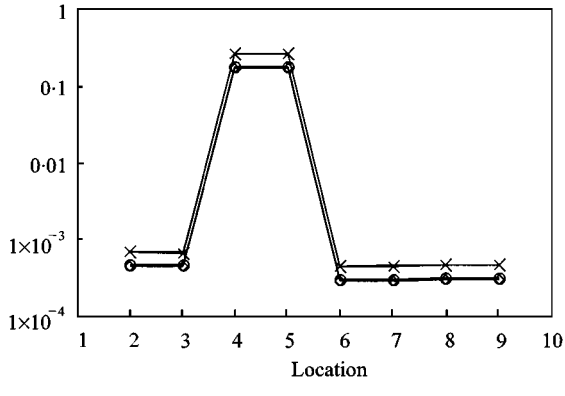

Figure 7. FRF curvature method for different localizations of input excitations. Keys: ——, 80% damage force co-ordinate = 1; -*-*-* 80% damage force co-ordinate = 3; —○—, 80% damage force co-ordinate = 7; -○-○-○, 80% damage force co-ordinate = 9.

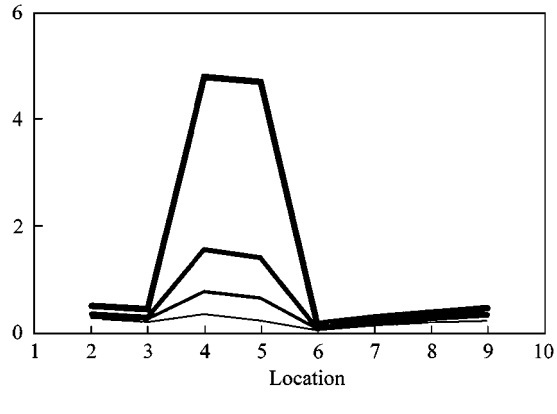

Figure 8. FRFs curvatures differnces for a frequency range of 0–50 rad/s. Input force at location 1. 10% of rms noise added to data. Keys: ——, 20% damage (between measurement points 4 and 5); ——, 40% damage (between measurement points 4 and 5); ▬, 60% damage (between measurement points 4 and 5); ▬, 80% damage (between measurement points 4 and 5).

3.2. THE FRF CURVATURE METHOD VERSUS THE MODE SHAPE CURVATURE METHOD

For this comparison the damage situation d1 (20% stiffness reduction) was considered and, as illustrated in Figure 9, the mode shape curvature method clearly indicates the damaged element and the results are better for higher order modes.

Figure 10 plots both methods normalized to 1 (all values were divided by the biggest one and it is clear that, for this example, the FRF curvature method has higher performance.

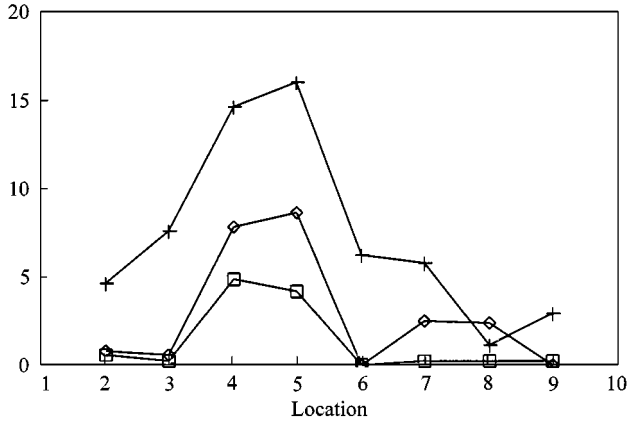

Figure 9. Mode shape curvature method (first three modes). Keys: —□—□ □, Mode 1 curvature difference (20% damage between the points 4 and 5); —◇—, mode 2 curvature difference (20% damage between the points 4 and 5); + — + — +, mode 3 curvature difference (20% damage between the points 4 and 5).

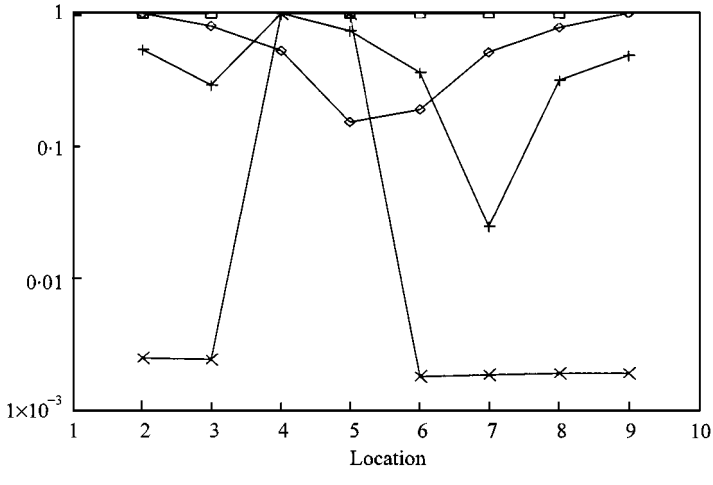

Figure 10. Comparison between the FRF and the mode shape curvature methods. Keys: —*—*—*, FRFs curvature difference (20% damage between the points 4 and 5); □—□ □, Mode 1 curvature difference (20% damage between the points 4 and 5); —◇—, mode 2 curvature difference (20% damage between the points 4 and 5); + — + — +, mode 3 curvature difference (20% damage between the points 4 and 5).

3.3. THE FRF CURVATURE METHOD VERSUS THE DAMAGE INDEX METHOD

For this comparison, the damage situation d1 (20% stiffness reduction) was also considered. The Damage index method clearly indicates the damaged element (see Figure 11).

From Figure 12, it is also clear, for this example, that the FRF curvature method was higher performance than the Damage index method.

4. EXPERIMENTAL EXAMPLE

Following previous work done by Charles R. Farrar and David V. Jauregui [7, 8] of Los Alamos National Laboratory (LANL), U.S.A. it was found important

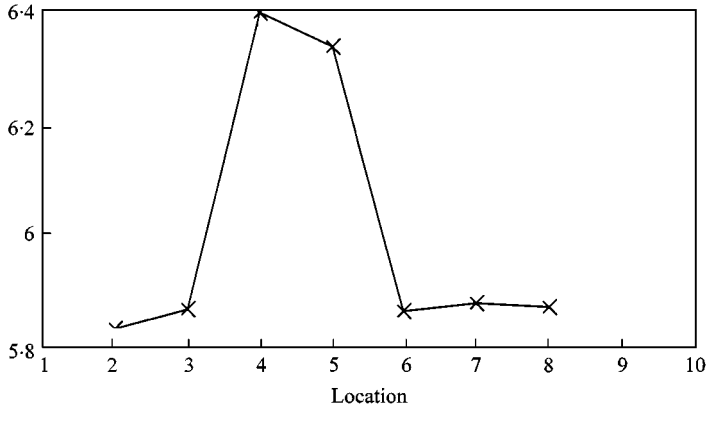

Figure 11. Damage index method (first six modes included). Keys: —×—×—×, Damage index, first six modes included (20% damage between the points 4 and 5).

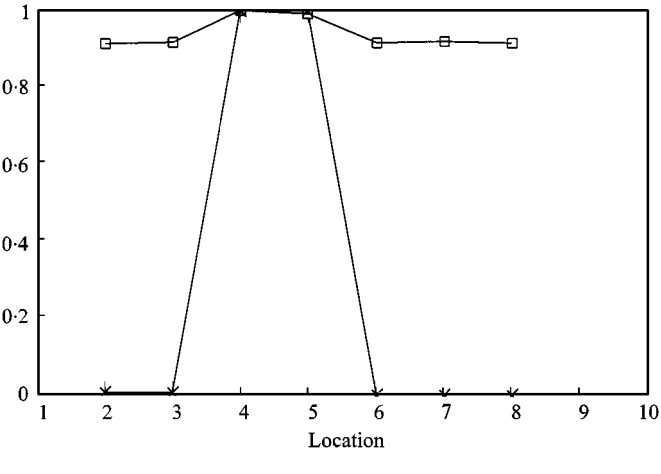

Figure 12. Comparison between the FRF curvature method and the Damage index method. Keys: —×—×—×, FRF's curvature differnce (20% damage between the points 4 and 5); —□—□—□, Damage index, first six modes included (20% damge between the points 4 and 5).

to the test the FRF curvature method, already tested numerically and expeimentally in beams, in a real large civil engineering structure, like the Interstate 40 (1–40) bridge over the Rio Grande in Albuquerque, NM, U.S.A. (Figure 13).

This bridge was to be razed during the summer of 1993. Investigators from the New Mexico State University obtained permission to destructively test the bridge prior to its removal and, with the help of LANL, were able to introduce cracks into the structure, simulating real possible damage situations, in order to test various damage identification methods using the experimental modal data.

The tested methods were the Damage index method, the Mode shape curvature method, the Change in flexibility method, the Change in uniform flexibility curvature method and the Change in stiffness method. All these methods require modal identification to determine amplitudes before and after the damage. The last three also require the resonant frequencies before and after the damage. As stated by Charles R. Farrar and David V. Jauregui the Damage index method performed the best.

The 1–40 bridge was built in early 1960s and is of twin 10-ft-deep plate-girder design, the three continuous spans being supported by concrete piers and abutment (Figure 14). The three lanes wide with concrete deck rest on plate girders and three stringers. Similar bridges have been found to develop fatigue cracks from the out-of-plane bending of the plate girder web (Figure 15).

Four levels of the damage (E-1, E-2, E-3 and E-4) were introduced to the middle span of the north plate girder close to the seat supporting the floor beam at midspan. Damage was introduced by making torch cuts in the web and the flange of the girder (Figure 16).

Figure 13. I-40 bridge over Rio Grande in Albuquerque, NM, U.S.A. (curtesy of Los Alamos National Laboratory).

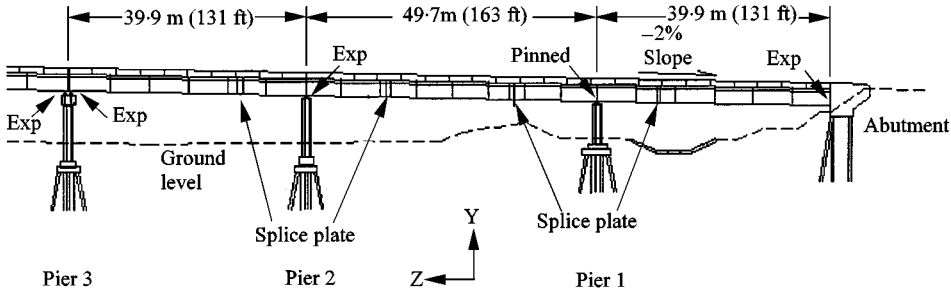

Figure 14. Elevation view of the portion of the tested I-40 bridge (courtesy of Los Alamos National Laboratory).

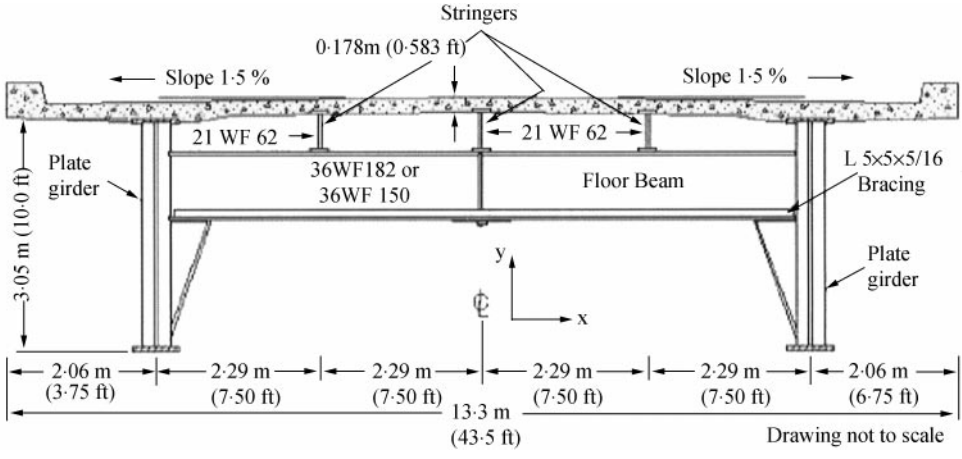

Figure 15. Cross-section geometry of the I-40 bridge (courtesy of Los Alamos National Laboratory).

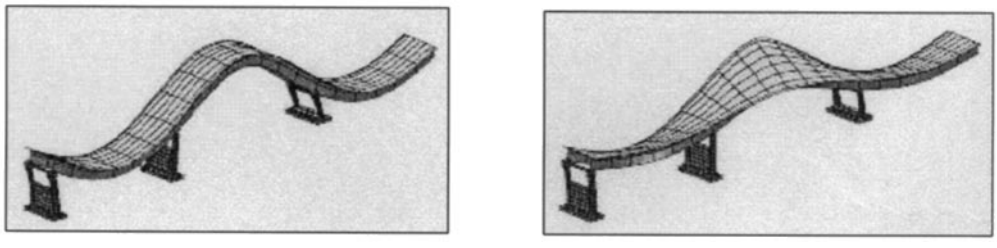

Figure 16. First flexural mode of the undamaged and damged bridge (courtesy of Los Alamos National Laboratory).

The FRFs were measured with 30 spectrum averages, frequency range of 0–12·5 Hz and frequency resolution of 0·03125 Hz. An hydraulic shaker was used to excite the bridge, above the south girder, midway between the abutment and first pier, with 2000-lb peak force random signal with frequency content between 2 and

10 Hz. Two rows of 13 accelerometers (sensitivity of 1 V/g) were mounted at mid-height of the north and south girders and equally spaced along the length of the span [7] (Figure 17).

To test our method with the bridge data, the FRFs measured on the north girder were used. The selected frequency range was 1·8–3 Hz to avoid the low-frequency noise and the higher frequency modes (see Figure 18). The damage was expected near the measurement location 7.

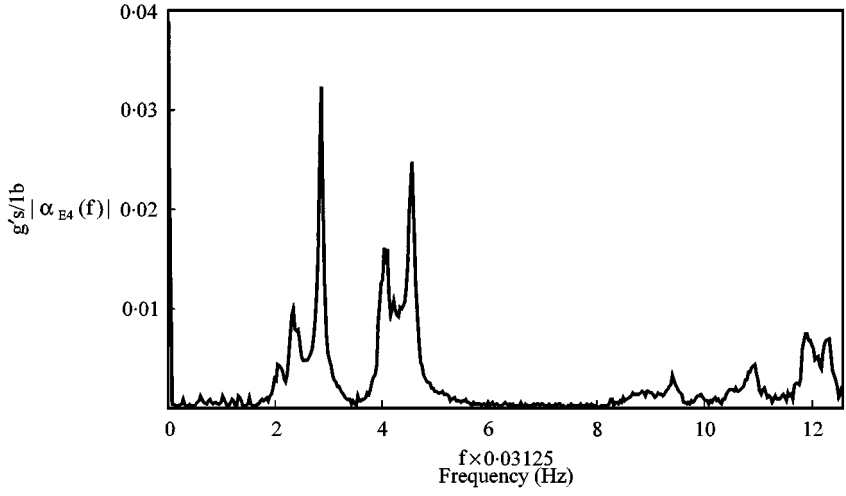

Figure 17. FRF measured at location 6 for the damage situation E-4 (linear amplitude scale).

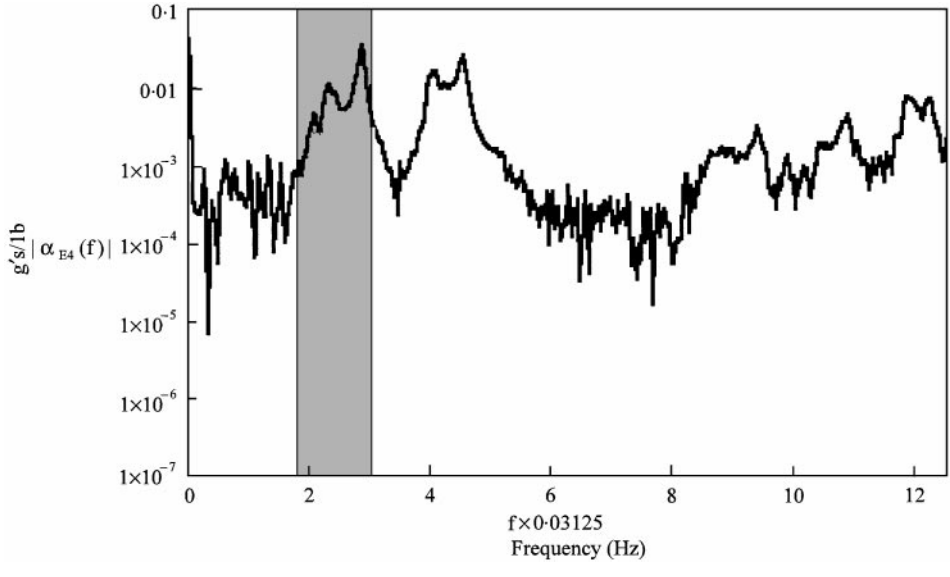

Figure 18. Frequency range selected to implement the FRF curvature method.

It is clear from Figure 19 that the method worked very well for the damage level 4 and, for the others, the damage detection was spread over two or three locations.

Figure 20 shows the results of the three methods for the damage scenario E-4. For better comparison they were normalized.

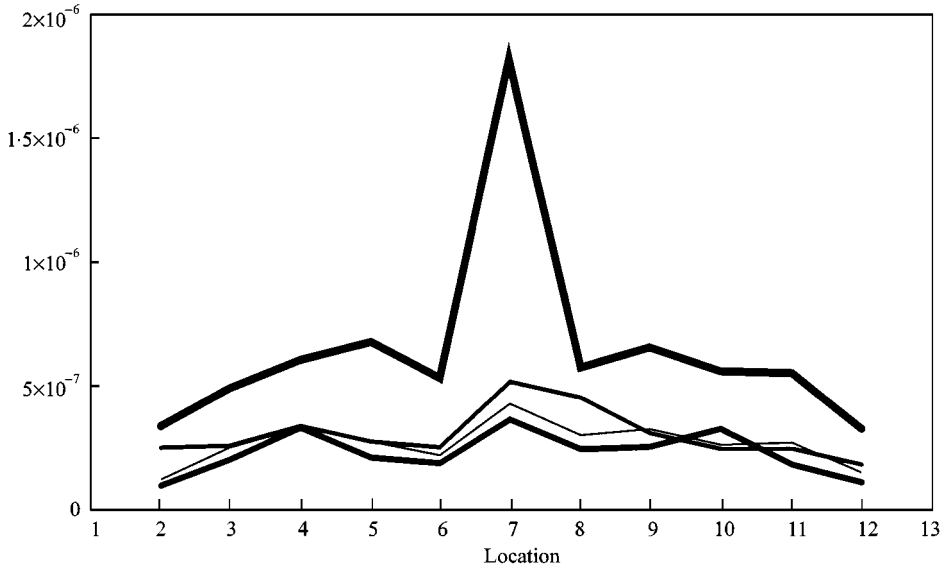

Figure 19. FRF curvature methods results to all the damage scenarios bridge data. Keys: ——, damage scanario E-1 (near location 7); ———, damage scanario E-2 (near location 7); ▬, damage scanario E-3 (near location 7); ▬, damage scenario E-4 (near location 7).

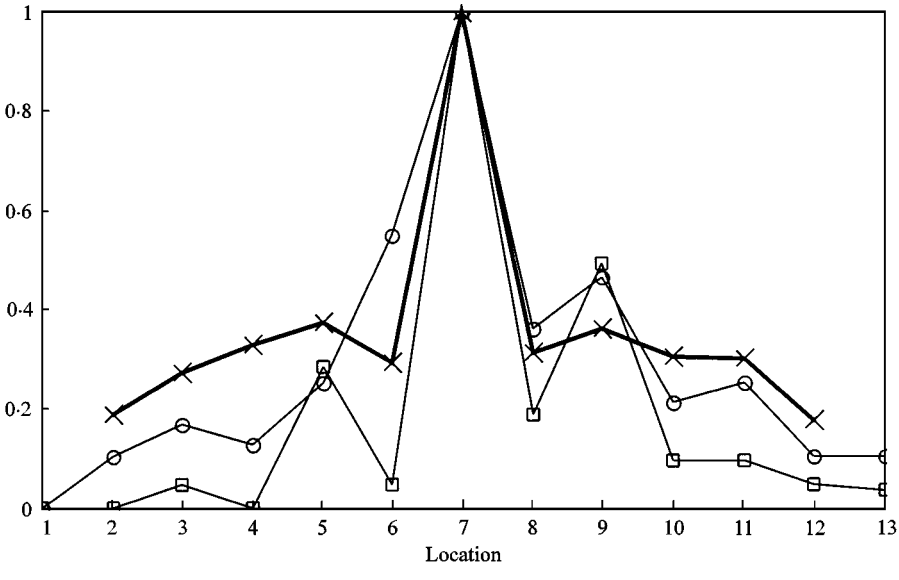

Figure 20. All the three methodd results to E-4 damage scenario bridge data. Keys: —×—×—×—, damage scenario E-4 (FRF Curvature Method); —□—□ □, damage scenario E-4 (damage Index Method); —○—○—○, damage scenario E-4 (Mode Shape Curvature Method).

5. SUMMARY AND CONCLUSIONS

The application of a new damage detection method using a numerical 10 d.o.f. lumped-mass system and the experimental data gathered from the I-40 bridge has been reported. In a way, this work can be understood as an addition to the previous papers of Farrar and Jauregui [7, 8] where they compared five linear damage identification methods using the same experimental data.

Results show that the FRF curvature method performed well in detecting, locating and quantifying damage, although this last item still has to be further developed and better characterized. Its main advantage is its simplicity and no need of performing a modal analysis for the identification of mode shapes or resonant frequencies, as is the case for the other methods.

ACKNOWLEDGMENTS

The authors would like to acknowledge Dr. Farrar and LANL for the authorization in using the photos and drawings of their work and for the I-40 bridge data, available through the internet on the LANL site.

REFERENCES

1. W. D. Scott, R. E. Charles, P. B. Michael and S. W. Daniel 1996 *Los Alamos LA-13070-MS*. Damage Identification and Health Monitoring of Structural and Mechanical Systems from Changes in Their Vibration Characteristics: A Literature Review.
2. R. E. Charles, W. D. Scott, C. Z. David and H. J. George III 1997 *XV International Modal Analysis Conference*. Orlando, U.S.A: SEM Course. Current horizons for structural damage detection.
3. N. M. M. Maia, J. M. M. Silva and R. P. C. Sampaio 1997 *XV International Modal Analysis Conference*. 942–946. Orlando, U.S.A. Localization of damage using curvature of the frequency-response-functions.
4. M. M. F. Yuen 1985 *Journal of Sound and Vibration* **103**, 301–310. A numerical study of the eigenparameters of a damaged cantilever.
5. A. K. Pandey, M. Biswas and M. M. Samman 1991 *Journal of Sound and Vibration* **142**, 321–332. Damage detection from changes in curvature mode shapes.
6. N. Stubbs, J. T. Kim and R. F. Charles 1995 *Proceedings XIII International Modal Analysis Conference*, Nashville, U.S.A. Field verification of a nondestructive damage localization and severity estimation algorithm.
7. V. J. David and R. F. Charles 1996 *Proceedings XIV International Modal Analysis Conference*, 1423–1429. Dearborn, U.S.A. Comparison of damage identification algorithm on experimental modal data from a bridge.
8. V. J. David and R. F. Charles 1996 *Proceedings XIV International Modal Analysis Conference*, 119–125. Dearborn, U.S.A. Damage identification algorithms applied to numerical modal data from a bridge.